PROTEINS: Structure, Function, and Genetics 5:313–321 (1989)

Molecular Dynamics Effects on Protein Electrostatics

John J. Wendoloski and James B. Matthew
E.I. du Pont de Nemours & Co., Central Research & Development Department, Experimental Station, Wilmington, Delaware 19880-0228

ABSTRACT **Electrostatic calculations have been carried out on a number of structural conformers of tuna cytochrome *c*. Conformers were generated using molecular dynamics simulations with a range of solvent simulating, macroscopic dielectric formalisms, and one solvent model that explicitly included solvent water molecules. Structures generated using the lowest dielectric models were relatively tight, with side chains collapsed on the surface, while those from the higher dielectric models had more internal and external fluidity, with surface side chains exploring a fuller range of conformational space. The average structure generated with the explicitly solvated model corresponded most closely with the crystal structure. Individual p*K* values, overall titration curves, and electrostatic potential surfaces were calculated for average structures and structures along each simulation. Differences between structural conformers within each simulation give rise to substantial changes in calculated local electrostatic interactions, resulting in p*K* value fluctuations for individual sites in the protein that vary by 0.3–2.0 p*K* units from the calculated time average. These variations are due to the thermal side chain reorientations that produce fluctuations in charge site separations. Properties like overall titration curves and pH dependent stability are not as sensitive to side chain fluctuations within a simulation, but there are substantial effects between simulations due to marked differences in average side chain behavior. These findings underscore the importance of proper dielectric formalism in molecular dynamics simulations when used to generate alternate solution structures from a crystal structure, and suggest that conformers significantly removed from the average structure have altered electrostatic properties that may prove important in episodic protein properties such as catalysis.**

Key words: protein, electron transfer, molecular dynamic simulations, dielectric

INTRODUCTION

Electrostatic interactions are implicated in every protein reaction that has an observable pH or ionic strength dependence. The dependencies of these reactions are usually attributed to the protein's net charge and asymmetries in the spatial distribution of its charged residues and/or Coulombic screening arising from counterions in the vicinity of the protein. A computational scheme for predicting electrostatic interactions in proteins[1–3] developed around the solvent accessibility modified Tanford–Kirkwood (SA-TK) macroscopic dielectric formalism has been shown to successfully predict diverse phenomena such as overall proton titration curves, individual site p*K* values, ion binding sites, midpoints for pH induced transitions, as well as pH and ionic strength effects on protein–protein[4–6] and protein–ligand interactions.[1,3] These computations require the X-ray coordinates of the protein and a dielectric model that relates an interaction energy with the spatial relationship of each pair of charge sites in the protein. In the SA-TK method, a solvent accessibility parameter is incorporated into the model for each protein charge site to allow for the irregularities of the protein–solvent interface.

A number of investigations have focused on a more rigorous treatment of the protein–solvent dielectric interface using the finite difference technique to account for the irregular dielectric boundary.[7–10] This method is proving to be a valuable tool in the theoretical understanding of the propagation of electric fields across irregular dielectric boundaries. Recent work has focused on demonstrating that this increase in rigor at the dielectric interface produces a good correspondence with protein p*K* perturbations and their ionic strength dependence.[9] The concept of using MD to generate alternate structures for evaluating the sensitivity of macromolecular computations to the assumption of a static crystal structure has only recently been addressed.[11,12]

To evaluate the implications of protein structural

Received December 27, 1988; revision accepted April 7, 1989.

Address reprint requests to J.B. Matthew, at his current affiliation, ICI Pharmaceutical Group, a business unit of ICI Americas INC., Wilmington DE 19897.

Abbreviations used: SA-TK, solvent accessibility modified Tanford–Kirkwood model; psec, picosecond (10^{-12} seconds); MD, molecular dynamics; RMS, root mean square; kT, a unit of thermal energy.

fluctuations, electrostatic calculations have been carried out on structures collected at selected time points along molecular dynamics (MD) trajectories of tuna cytochrome *c*. Individual p*K*, overall titration curves, and electrostatic potential surfaces were calculated for each time point using the SA-TK algorithm. Since the details of the calculated structures depend on the dielectric formalism in the nonbonded electrostatic term of the MD potential function, five different simulations have been carried out: four using macroscopic, solvent-simulating, dielectric formalisms, and one that explicitly included solvent water molecules. Comparisons of electrostatic properties are reported between the crystal structure and the average structures derived for each trajectory.

COMPUTATIONAL METHODS

Molecular dynamics simulations have been carried out on tuna cytochrome c[13–15] using the Program AMBER[16,17] coupled to GEMM[18] on an ST100 array processor. The charge distribution on the protein titratable sites was assigned to correspond to cytochrome *c* at neutral pH, 7.0. Trajectories were computed with five different dielectric models for *D* in the nonbonded electrostatic term

$$E_{ij} = Q_iQ_j/DR_{ij}$$

of the potential function. R_{ij} is the charge site separation between centers i and j and Q_i is the charge on center i. The dielectric formalisms include two low dielectric models with *D* equal to R_{ij} (*DR*) and $4R_{ij}$ (*D4R*), two high dielectric, implicit solvent-simulating, models with *D* equal to 50 (*D*50) and 80 (*D*80), and a high dielectric model where *D* is set equal to 1 and 800 explicit TIP3P[19] water molecules are included (*D*W). The computations were carried out with a femtosecond time step and a coordinate set was saved every 50 fsec. The simulations were run for 100 psec (postequilibration) yielding 2000 coordinate data sets per run.

An average structure was computed for each of the dynamic simulations from the atomic coordinates of the data sets along the trajectory. The average structures were calculated as the average of the cartesian coordinates for each atom over the last 2000 structures (100 psec) of the simulation. This generates structures where each atomic position corresponds to a conformational population average and the contribution of each conformer is weighted by the probability of its occurrence in the simulation. This is analogous to the population averaging that occurs in crystal structure determinations. Individual structures along the trajectories were also studied to explore the range of unique conformations accessible to the protein on the picosecond timescale. For each of the average structures and a sampling of structures taken at time points along the trajectories, the solvent-accessible surface area was calculated[20] and an iterative electrostatic calculation[2] was carried out to predict the effective p*K* value for all titrable sites from pH 2.0 to 12.0 at ionic strengths of 0.01 and 0.1. The overall titration curves and electrostatic stability as a function of pH were also calculated.[21] In these computations the assumption is made that the structures generated in the trajectories at pH 7.0 are valid over the pH range reported. The electrostatic potentials about the protein structures were calculated at pH 7.0, $I = 0.01$ and 0.1 on a 1 Å orthogonal lattice by procedures and programs described elsewhere.[1,2,22]

TABLE I. RMS Difference Between the Average Structures and the Crystal Structure*

Simulation+	α-Carbon atoms	All atoms	Side chains atoms
DR	1.58	2.09	2.36
D4R	1.54	2.00	2.25
*D*50	1.27	1.56	1.73
*D*80	1.87	2.28	2.50
*D*W	0.93	1.20	1.36

*Average structure was computed for each dynamic simulation from the 2000 postequilibrium data sets collected along the trajectory.

+*DR*, *D4R*, *D*50, *D*80, *D*W refer to the dielectric formalisms used in the five simulations; with D = *R*, (4*R*), 50, 80, 1 with 800 explicit solvent molecules.

RESULTS

Generation of Alternative Structures

In Table I the 100 psec average structures for the five MD trajectories with the crystallographically determined, also time average, structure are compared. Root mean square (RMS) differences in atomic positions are given for α-carbon positions, all atom, and side chain positions. Historically, computed thermal factors for side chain and or backbone atoms (B-values) have been compared to crystallographicly determined B-values as a criteria for validating a MD trajectory. RMS differences, reported here in angstroms, are a more quantitative approach. B-value comparisons, not reported here, are in qualitative agreement with the RMS difference comparisons. The simulation whose structure agrees most closely with the atomic positions in the crystal structure in all three cases is *D*W, the uniform dielectric of one with the explicit inclusion of water. Of the macroscopic dielectric trajectories, *D*50 corresponds most closely to the crystal structure and the explicit water simulation. Higher and lower uniform dielectric simulations differ more in both main chain and side chain positions compared to the crystal structure or the more realistic water simulation. In agreement with the observation of Northrup et al.,[23] the surface side chains collapsed or laid down on the protein surface early in the low in vacuo dielectric (*DR*, *D4R*) trajectories. The charged side

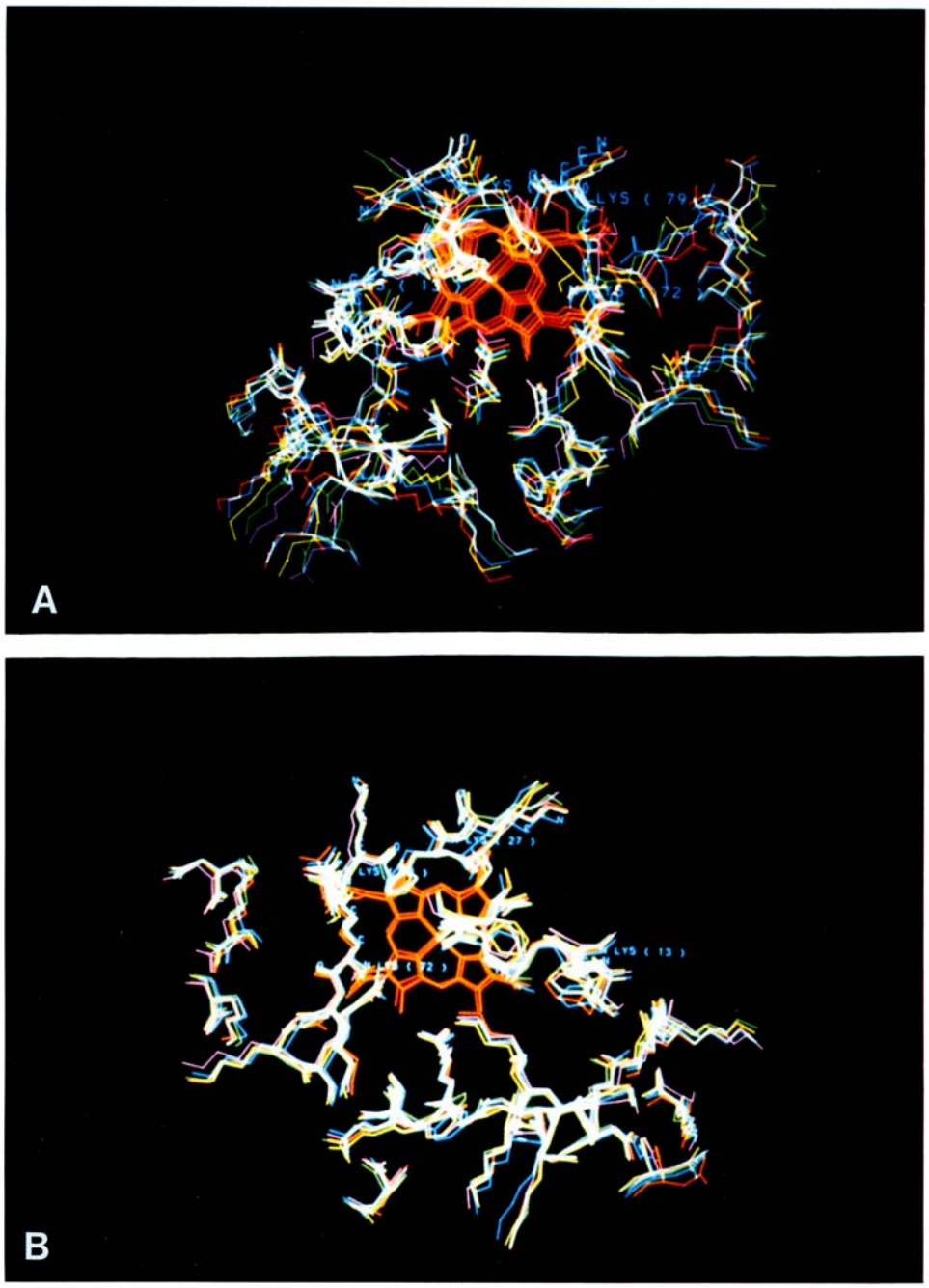

Fig. 1. Heme face view of cytochrome *c* superpositions of five coordinate sets taken along the trajectory for the **A,** high dielectric (*D*80) and **B,** solvated protein (*D*W).

chains formed ion pairs or disrupted secondary structure by hydrogen bonding to main chain N-H or C = 0 groups. Subsequent charged side chain reorientations in the low dielectric simulations were minimal. In the high dielectric trajectories with solvent implicitly or explicitly included (*D*50, *D*80, and *D*W), the side chains remained extended from the protein surface and underwent frequent thermal and collisional reorientations. Figure 1 shows the superposition of five structures taken at 1 psec intervals along the *D*80 (1a) and *D*W (1b) trajectories. In the case where water molecules were explicitly included (*D*W), the side chain behavior was similar to that in the macroscopic dielectric simulations, but was modulated or damped by the effect of the solvent viscosity. Over a longer time period the side chains

TABLE II. Ion Pairs, Solvent Accessible Surface, and Molecular Volume

Simulation[+]	Ion pairs* Number	$\bar{r}_{ij}$ (Å)	SA[‡] (Å^2)	Volume (Å^3)
DR	14	2.7	4999	17960
D4R	14	2.9	5302	18710
*D*50	4	3.5	5540	18731
*D*80	5	3.5	5512	18915
*D*W	2	3.0	6054	19546
X-ray	1	3.3	5914	19158

*Refers to the number of ion pairs observed in the average structure for each simulation with an interatomic distance of 3.8 Å or less; and r_{ij} refers to the average of the individual ion pair distances.

[+]*DR, D4R, D*50, *D*80, *D*W refer to the dielectric formulations used in the five simulations; with D = *R*, (4*R*), 50, 80, 1 with 800 explicit solvent molecules.

[‡]Static solvent accessibility.

in the *D*W trajectory sampled the same range of conformational space as observed in the more rapidly diffusing *D*50 and *D*80 simulations.

In Table II, the number of ion pairs or salt bridges for the average structure from each trajectory is reported and compared with the corresponding average interatomic distance in the crystallographic structure. The abundance of ion pairs with short interatomic distances in the low dielectric simulations is indicative of the dominating effect of the unscreened Coulombic interaction. In the higher dielectric simulations, the number of salt bridges and their average length are more consistent with the ion pair pattern in the X-ray structure. The total solvent-accessible surface area and calculated volumes are also included in Table II. This volume includes all the space within the protein's solvent accessible surface as defined by a 1.4 Å probe. Taken together, the reduced surface areas and volumes indicate a contraction at the protein surface in the low dielectric trajectories that is not evident in the trajectories that include a high dielectric, solvent-simulating formalism. Surface areas and volumes fluctuate along each trajectory ±200 Å^2 and ±150 Å^3, respectively. Eden et al.[24] reported the RMS volume fluctuations, approximated from an ideal solution treatment of compressibility data, for ferrocytochrome *c* to be 74 Å^3. The RMS volume fluctuations deduced from the dynamic simulations ranged from 50 to 115 Å^3, with the more realistic solvent shell simulation giving 85 Å^3.

ELECTRODYNAMICS

Individual site p*K*

At a given pH, the protein's unique spatial distribution of charge sites confers an effective proton affinity on each titrable site. This effective p*K* is determined by the interplay of the protein's entire charge complement. The effective p*K* value is defined at each pH as the deviation from the intrinsic p*K* given by the electrostatic interaction free energy summed over the protein charge array. Since the effective p*K* values of every charge site is found to vary with pH, it is convenient to refer to the $pK_{1/2}$ value, the pH at which a particular group is half titrated. The Coulombic influence on a site *i* exerted by each site *j* (i.e., the $\blacktriangle pK_{ij}$) is proportional to the charge at the *j*th site and the extent of its burial within the protein, and inversely proportional to the intercharge distance R_{ij}. The prediction of how p*K* values (and therefore the fractional charge *Z*) for each site will vary with alternative side chain orientations (and therefore alternative charge site separations) is critical to understanding the charge site interplay that gives rise to the diverse pH and ionic strength effects observed in proteins. In figure 2, the acidic residue $pK_{1/2}$ values calculated on the average structures from the *DW, D*80, and *DR* trajectories are plotted against the calculated $pK_{1/2}$ values for the crystal structure. Both solvent-simulating trajectories give rise to average structures that compare equally well with the crystal structure, but the electrostatic interactions in the time average structure from the *DR* trajectory are markedly different. The correlation coefficients are 0.77, 0.79, and 0.20, respectively. In general the low dielectric structure has a preponderance of salt bridges that give lower p*K* values for the acidic functions (Fig. 2B). There is good overall agreement in the solvent simulating cases (Fig. 2A). The few p*K* differences can be traced to structural differences between the simulation average structures and the crystal structure. For example, Asp-50 is predicted to have a p*K* of 3.8 and 3.9 in the simulated structures and 2.6 in the crystal structure. In the crystal structure Asp-50 is in a salt bridge that is predicted to be, on average, broken in both solvent simulations. Other less dramatic differences suggest more subtle differences in protein structure between the crystal structure and the simulated average solution structures. If the Asp-50 salt bridge is considered a legitimate solution-crystal structure difference, the correlation coefficients for Figure 2A are 0.93 and 0.98. Figure 3 shows the calculated range of $pK_{1/2}$ values for the titrable sites in cytochrome *c* that are predicted to reach their titration midpoint between pH 2 and pH 11. In Figure 3A and B the $pK_{1/2}$ values are reported for the titrable acidic and basic functions, respectively, for individual structural conformers collected along the *D*80 and *D*W trajectories. The dependence of the $pK_{1/2}$ on allowed alternative protein conformers has direct bearing on the significance one might place on the correspondence between an experimental p*K* value and a p*K* predicted for a single conformer (i.e., the X-ray structure). In general, the p*K* fluctuation is highly dependent on each charge site's unique environment, with some groups (in broad electrostatic potential wells) having little structural

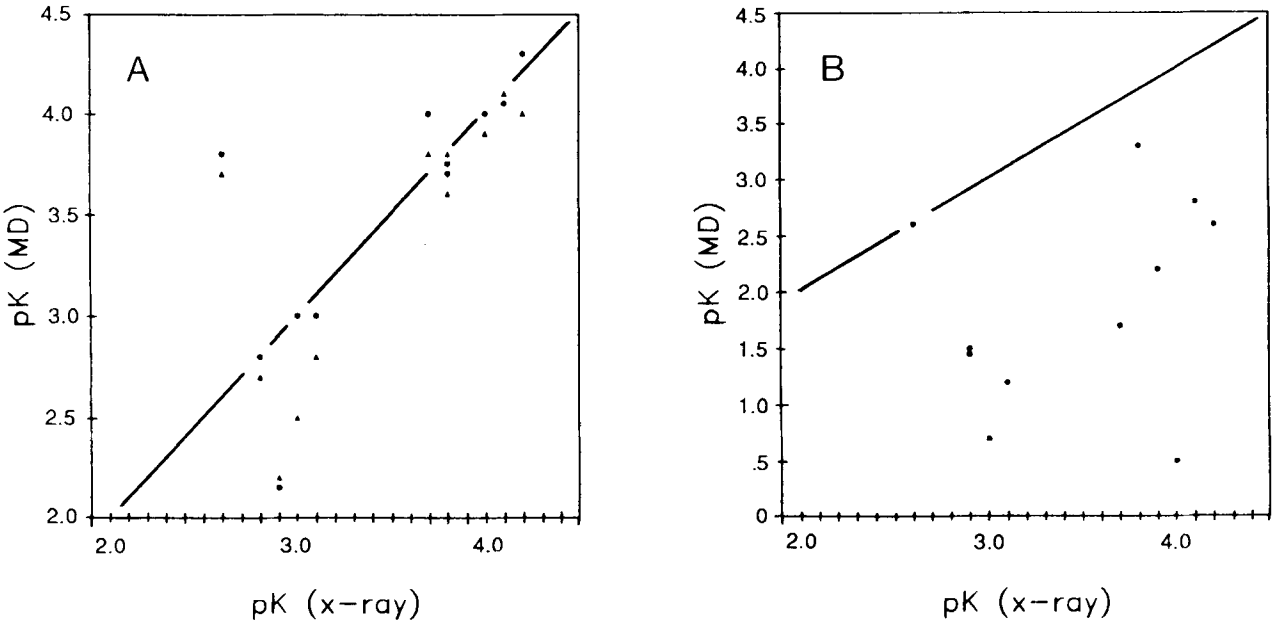

Fig. 2. Comparison of computed $pK_{1/2}$ for the acid residues of cytochrome *c*. **A:** Comparison of $pK_{1/2}$ values computed from the *D*W explicit solvent (●) and *D*80 uniform dielectric of 80 (▲) with those computed from the crystal structure. **B:** Dielectric equal to charge separation.

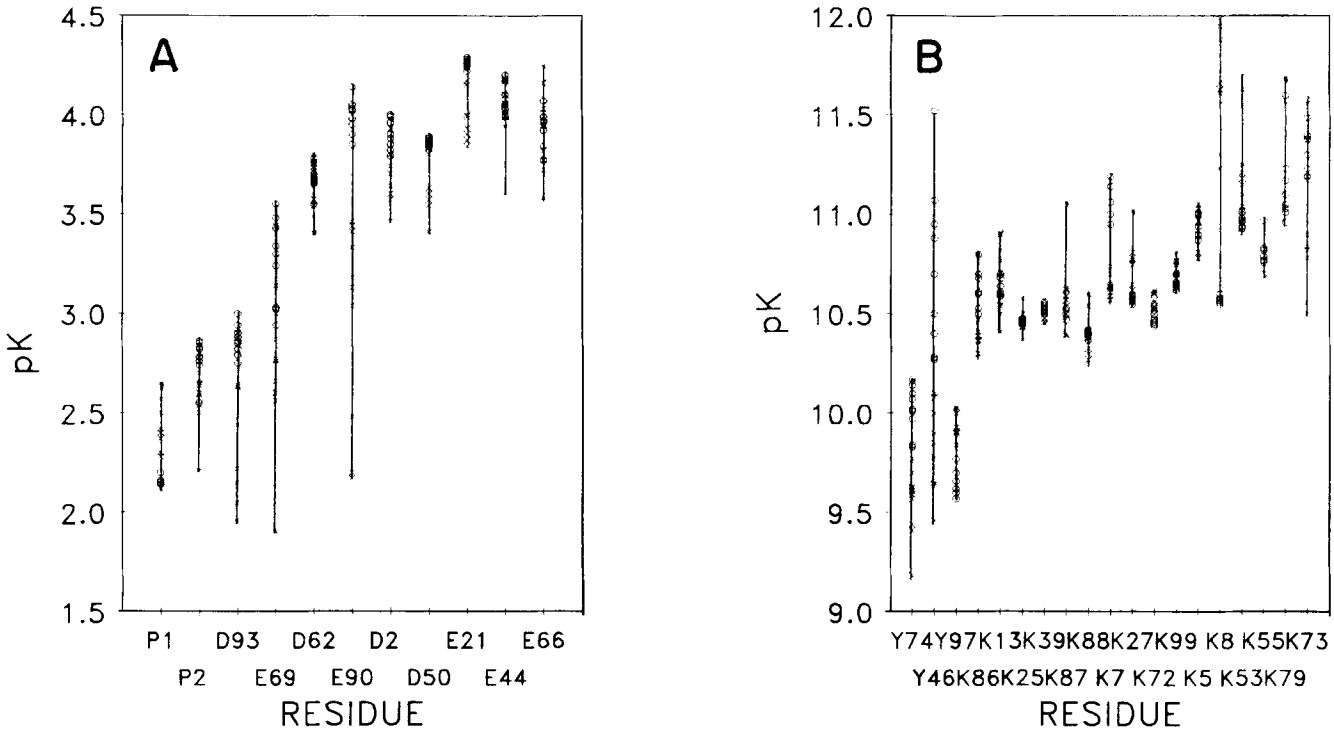

Fig. 3. Variation of calculated $pK_{1/2}$ values at 0.01 ionic strength for cytochrome *c* structures taken from the uniform dielectric of 80 (*D*80) and the explicit water simulations (*D*W); (**A**) acidic residues and (**B**) basic residues whose titration midpoints fall between pH 2.0 and 11. p*K* values are plotted for 20 structures, 10 structures from the *D*W (○) and 10 from the *D*80 trajectories (×). *X*-axis labels refer to single amino acid code and residue number; P1 and P2 refer to heme proprionates.

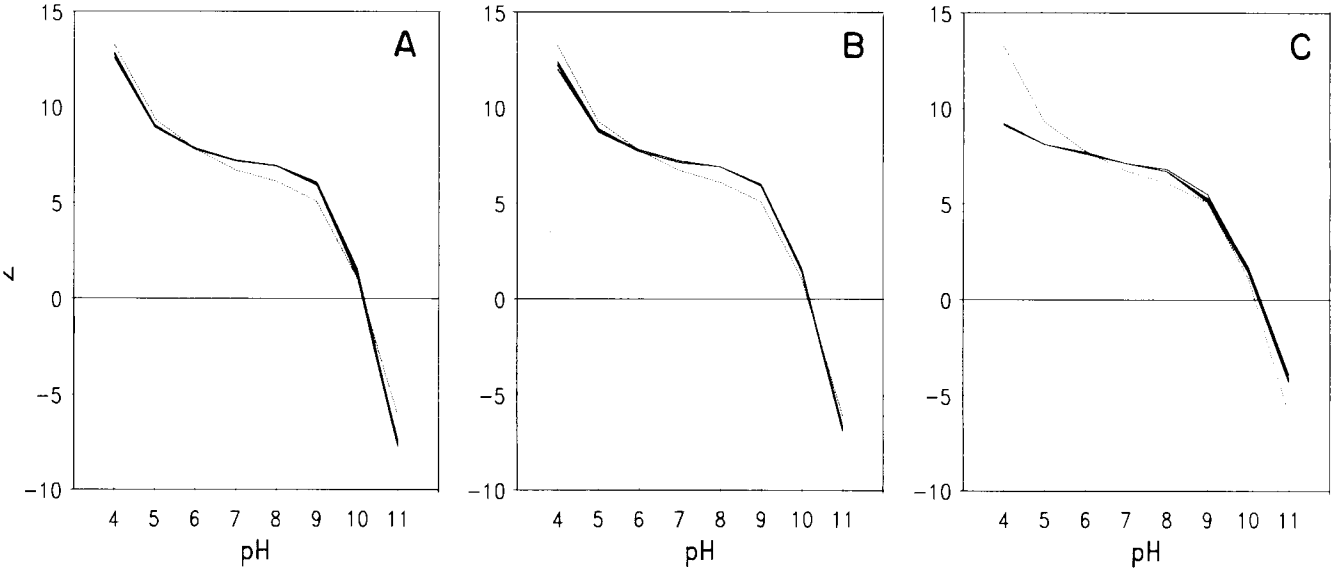

Fig. 4. Comparison of the experimental (dotted curve) and predicted protein net charge (z) (solid curves), at 0.1 ionic strength, for ten structures taken along the (**A**) explicit water (*D*W), (**B**) the uniform 80 dielectric (*D*80) simulations, and (**C**) the distance dependent $4R_{ij}$ (*D4R*).

dependence in their pKs, while other sites have fluctuations up to ±1.0 pK unit. The range of pK values shown in Figure 3 is indicative of calculated values for structures from all three high dielectric, solvent-simulating trajectories.

Overall Titration Curves

The theoretical titration curves were constructed by summing the predicted fractional charge for each site at each pH. The titration curves for structures taken along the *D*W, *D*80, and *DR* trajectories are compared with the experimental titration curve for cytochrome *c* in Figures 4A, B, and C, respectively. The experimental titration curve is relatively flat in the neutral pH range where the single free histidine titrates, and has a strong pH dependence at acid pH where 12 carboxyls (four aspartate, five glutamate residues, the C-terminus, and two proprionates) protonate, and at basic pH where 23 sites (16 lysine, two arginine, and five tyrosine residues) deprotonate. The predicted titration curves for structures along the same trajectory are indistinguishable even though there is considerable variation in the individual site $pK_{1/2}$ values between structures (Fig. 3). The titration behavior predicted for the *D*W and *D*80 structures agrees equally well with experiment, but the structures from the DR in vacuo trajectory give titration curves that differ from the experimental determination in the acidic and basic regions. Essentially, the low dielectric *DR* formalism gives structures that have acidic and basic side chain pK values shifted to lower and higher pH, respectively, due to the preponderance of ion pairs (Table II).

Electrostatic Stabilization

The pH dependent electrostatic free energies at 0.1 ionic strength, determined as the sum of all pairwise interactions between charge sites, are shown in Figure 5 for structures along the *DR*, *D*80, and *D*W trajectories. The lower curves are from the *DR* structures and the upper curves are calculated from the *D*W and *D*80 structures. The structures generated with the explicit and implicit solvent simulating dielectric again give similar results, while the low dielectric, ion paired structures give stability curves that are about 9 kcal/mol higher over the entire pH range.

Potential Surface Fluctuation

In Figure 6, calculated electrostatic potential surfaces at 3 kT and 4 kT are shown for two cytochrome *c* structures taken at 1 psec intervals along the *D*80 trajectory. These equipotential surfaces were calculated at pH 7.0, 0.01 ionic strength. In cytochrome *c* the area of highest positive potential is centered about the heme crevice with extensive shells of decreasing potential being more removed from the protein surface. In Figure 7, the volume of the electrostatic isopotential energy shells (at ionic strengths of 0.01 and 0.1 pH 7.0) is given for 10 structures taken from the *D*80 trajectory. Each volume includes only that volume outside the structure's solvent accessible surface area. The structures from the *D*W, *D*50, and *D*80 trajectories also give curves that fall within the range shown. The largely positive potential reflects the protein's net positive charge at this pH, with the areas of highest positive potential

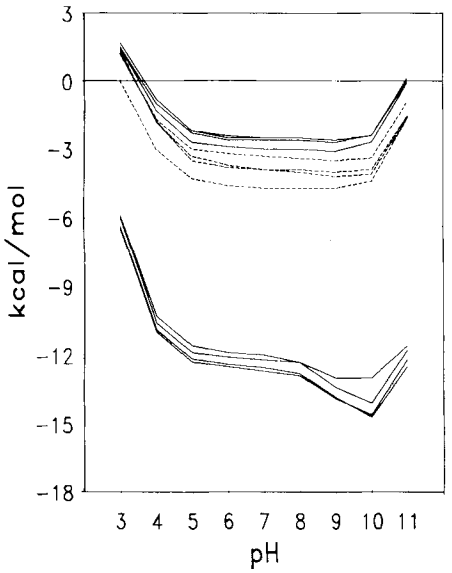

Fig. 5. Calculated pH dependent stability for structures taken along the *D*80 (broken lines) and the *DW* (upper-solid) and the *DR* (lower-solid) trajectories at 0.1 ionic strength.

being close to or at the protein solvent-accessible surface near the heme edge.[6,25] The extent of the positive and negative potential surfaces around cytochrome *c* fluctuates substantially with side chain reorientation. At an ionic strength of 0.01 the volume of the +2 kT isopotential shell varied from 14,800 to 16,000, the +3 kT from 2,400 to 3,400, the +4 kT from 400 to 600 Å^3 etc. (Fig. 7). The volume shell around the protein at each potential has a corresponding local concentration of counterions determined as

$$C_{\text{local}} = C_{\text{bulk}}e^{\psi}$$

where ψ is the potential in units of kT and C_{local} and C_{bulk} are the local and bulk ion concentrations. Therefore, the volume with +2 kT is predicted to have a counterion concentration seven times the bulk solvent concentration and the +5 kT volume corresponds to 150 times the bulk or local ion concentrations in excess of one molar at the protein surface. The electrostatic potential of individual structures (when averaged) resembles the average structure potential map, but transient high potential sites are predicted that could facilitate charged substrate association and/or play a role in a catalytic event.

DISCUSSION

For many years, the fundamental assumption made in nearly all electrostatic calculations has been that of a static structure. The fact that computations based on crystal structures have been very successful in predicting protein pH and ionic strength-dependent properties supports the general correspondence between protein crystal and solution structures. Attempts to improve electrostatic computational techniques for macromolecules is currently an area of intense study. For example, a recent study compared the observed ionic strength dependence of a single histidine p*K* in subtilisin with values calculated with 14 variations on handling the protein–solvent boundary with macroscopic formalisms.[8,9] Because of the dynamic aspects of protein structure and its consequences for protein activity and function[11] it is necessary to consider what protein properties are best computed by using a time average structure (like the crystal structure) and what protein properties require a consideration of the extremes in the structural conformer distribution. The present results (Figure 2A) show that two different time average structures (crystal and *DW* simulation or *DW* and *D*80 simulations) give rise to predicted p*K* values that differ on average by 0.18 p*K* units. While the predictions for some residues are identical, others differ by more than one log unit. This implies that unless the complications of side chain fluidity are adequately taken into account, it will not be possible to differentiate between electrostatic models that predict p*K* values or p*K* perturbations wtihin a few tenths of the experimental p*K*. In one study[26] where 80 histidine p*K* values from 12 different myoglobins were measured and compared to computed p*K* values, the correlation coefficients were 0.94 to 0.99 for the various species even though individual sites differed by 0.5 p*K* units from the experimental. Interestingly, one of the largest differences in predicted versus observed p*K* was for a histidine that modification studies (solution and crystal) and NMR studies clearly showed was in an ion pair in solution that was broken in the crystal structure. This is the converse to the computations prediction that the Asp-50 ion pair is broken in solution compared to the crystal structure.

While side chain conformational flexibility has effects on local electrostatic interaction such as p*K* values, it does not necessarily affect the concept of electrostatic preorientation in macromolecular docking reactions provided an adequate dielectric model is used. Examples of successful modeling of docking reactions include protein–protein electron transfer complexes,[4–6,25] protein–protein electron transfer facilitated diffusion,[27] and protein–DNA complexes.[28,29] These studies have typically used overlap of complementary electrostatic potentials, calculated for static structures, as the criteria for defining the best complexes. However, molecular dynamic simulations carried out on a docked electron transfer complex have shown that the details of the final phase of docking is dependent on charged side chain fluctuations.[11] This raises the question of why the conformational flexibility and the changes in electrostatic potential affect the local vs preorientation and facilitated diffusion cases differently. In the

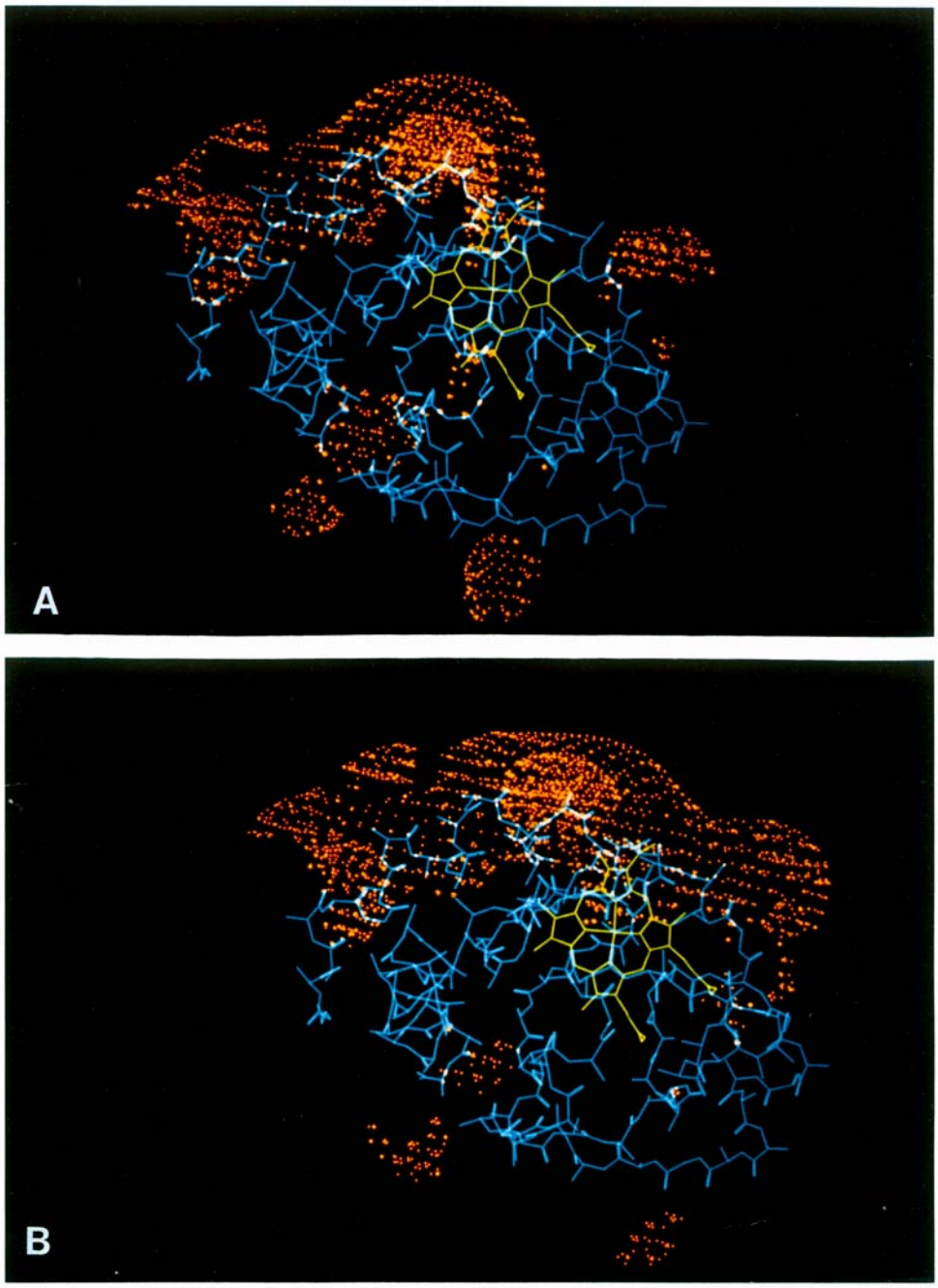

Fig. 6. Calculated electrostatic potential surfaces for two structures taken at 1 psec intervals along the high dielectric, *D*80, trajectory. Shown are the 3 kT (outer) and 4 kT (inner) surfaces calculated at pH 7.0, 0.01 ionic strength.

more realistic dielectric simulations (*D*50, *D*80, and *D*W), the side chains remain predominantly extended from the surface and undergo random orientations. In the preorientation phase of the docking reactions, an incoming protein would feel the long range, low kT potentials with their fluctuations being averaged on the timescale of protein diffusion. As the docking progresses to shorter separation distances (less than 10 Å) the potentials intensify, protein diffusion is enhanced, and the fluctuating higher kT potentials will become relevant in steering the incoming molecule into alternate docked geometries or may facilitate migration over the protein surface.[11,27] These results indicate that while low dielectric in vacuo models are not valid for systems in which surface electrostatic interactions are im-

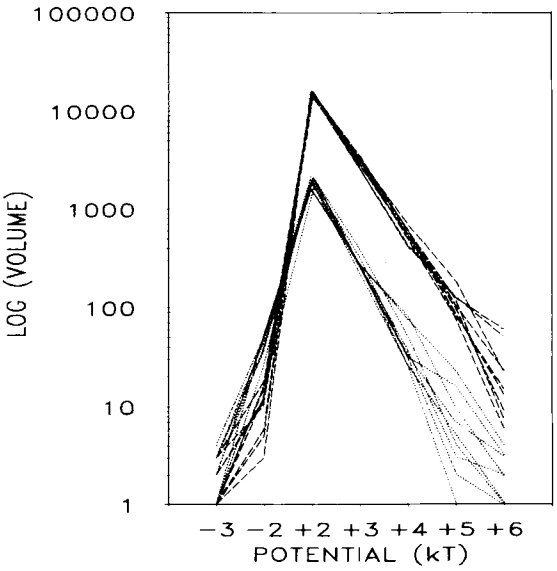

Fig. 7. Volume in cubic angstroms of the electrostatic isopotential shells around cytochome *c* for structures taken along the *D*80 trajectory at pH 7.0, ionic strengths of 0.01 and 0.1 (broken lines and dotted lines, respectively).

portant, a high dielectric formalism such as *D*50 or *D*W may be adquate in modeling preorientation of facilitated diffusion docking reactions with static structures.

ACKNOWLEDGMENTS

The authors would like to thank Dr. F.R. Salemme and Dr. S.H. Northrup for helpful discussion.

REFERENCES

1. Matthew, J.B., Gurd, F.R.N. Calculation of electrostatic interactions in proteins. Methods Enzymol. 130:413–455, 1986.
2. Matthew, J.B. Electrostatic effects in proteins. Annu. Rev. Biophys. Biophys. Chem. 14:387–417, 1985.
3. Matthew, J.B., Richards, F.M. Anion binding and pH-dependent electrostatic effects in ribonuclease. Biochemistry 21:4989–4999, 1982.
4. Matthew, J.B., Weber, P.C., Salemme, F.R., Richards, F.M. Electrostatic orientation during electron transfer between flavodoxin and cytochrome c. Nature (London) 301:169–171, 1983.
5. Weber, P.C., Tollin, G. Electrostatic interactions during electron transfer reactions between c-type cytochromes and flavodoxin. J. Biol. Chem. 260:5568–5573, 1985.
6. Mauk, M.R., Mauk, A.G., Weber, P.C., Matthew, J.B. Electrostatic analysis of the interaction of cytochrome c with native and dimethyl ester heme substituted cytochrome b_5. Biochemistry 25:7085–7091, 1986.
7. Warwicker, J., Watson, H.C. Calculation of the electric potential in the active site cleft due to α-helix dipoles. J. Mol. Biol. 157:671–679, 1982.
8. Gilson, M.K., Honig, B.H. Calculation of electrostatic potentials in an enzyme active site. Nature (London) 330;84–86, 1988.
9. Gilson, M.K., Honig, B.H. Energetics of charge-charge interactions in proteins. Proteins 3:32–52, 1988.
10. Gilson, M.K., Sharp, K.A., Honig, B.H. Calculating the electrostatic potential of molecules in solution: Method and error assessment. J. Comput. Chem. 9:327–335, 1987.
11. Wendoloski, J.J., Matthew, J.B., Weber, P.C., Salemme, F.R. Molecular dynamics of a cytochrome c-cytochrome b_5 complex. Science 238:719–797, 1987.
12. Wendoloski, J.J., Matthew, J.B. Time dependent fluctuation of tuna cytochrome c: Effect of dielectric function. Biophys. J. 53:113, 1988.
13. Takano, T., Dickerson, R.E. Conformation change of cytochrome c. Ferricytochrome c structure refined at 1.5Å resolution. J. Mol. Biol. 153:79–94, 1981.
14. Takano, T., Dickerson, R.E., Conformation change of cytochrome c: Ferricytochrome c refinement at 1.8Å and comparison with the ferrocytochrome structure. J. Mol. Biol. 153:95–110, 1981.
15. Bernstein, F.C., Koetzle, T.F., Williams, G.J.B., Meyer, E.F., Jr., Brice, M.D., Rodger, J.R., Kennard, O., Schimanouchi, T., Tasume, M.J. The protein data bank: A computer-based archival file for molecular structures. J. Mol. Biol. 112:535–542, 1977.
16. Weiner, P., Kollman, P.A. AMBER: Assisted model building with energy refinement. A general program for model molecules and their interactions. J. Comput. Chem. 2:287–299, 1981.
17. Weiner, S.J., Kollman, P.A., Case, D.A., Singh, U.C., Ghio, C., Alagona, G., Weiner P. A new force field for molecular mechanical simulation of nucleic acids and proteins. J. Am. Chem. Soc. 106:765–784, 1984.
18. Brooks, B.R. Applications of molecular dynamics for structural analysis of proteins and peptides. In: Supercomputer Research in Chemistry and Chemical Engineering," C. Jensen and D. Truhlar, eds. American Chemical Society, 1987: 123–145.
19. Jorgensen, W.L., Chandrasekhar, J., Madura, J., Impey, R.W., Klein, M.L. Comparison of simple potential functions for simulating liquid water. J. Chem. Phys. 79:926–935, 1983.
20. Lee, B.K., Richards, F.M. The interpretation of protein structure: Estimation of static accessibility. J. Mol. Biol. 55:379–400, 1971.
21. Matthew, J.B., Friend, S.H., Botelho, L.H., Lehman, L.D., Hanania, G.I.H., Gurd, F.R.N. Discrete charge calculations of potentiometric titrations for globular proteins: Sperm whale Mb, hemoglobin alpha chain, cytochrome c. Biochem. Biophys Res. Commun. 81:416–421, 1978.
22. Wensel, T.G., Meares, C.F., Vlachy, V., Matthew, J.B. Distribution of ions around DNA, probed by energy transfer. Proc. Natl. Acad. Sci. U.S.A. 83:3267–3271, 1986.
23. Northrup, S.H., Pear, M.R., Morgan, J.D., McCammon, J.A. Molecular dynamics of ferrocytochrome c. Magnitude and anisotropy of displacements. J. Mol. Biol. 153:1087–1109, 1981.
24. Eden, D., Matthew, J.B., Rosa, J.J., Richards, F.M. Increase in apparent compressibility of cytochrome c upon oxidation. Proc. Natl. Acad. Sci. U.S.A. 79:815–819, 1982.
25. Salemme, F.R. Structure and function of cytochrome c. Annu. Rev. Biochem. 46:299–329, 1977.
26. Botelho, L.H., Friend, S.H., Matthew, J.B., Lehman, L.D., Hanania, G.I.H., Gurd, F.R.N. Protein NMR studies of histidine-ionizations in myoglobins of various species. Comparison of observed and computed pK values. Biochemistry 17:5197–5205, 1978.
27. Northrup, S.H., Boles, J.O., Reynolds, J.C.L. Brownian dynamics of cytochrome c and cytochrome c peroxidase. Science 241:67–70, 1988.
28. Matthew, J.B., Ohlendorf, D.H. Electrostatic deformation of DNA by a DNA-binding protein. J. Biol. Chem. 260: 5860–5862, 1985.
29. Steitz, T.A., Weber, I.T., Matthew, J.B. Catabolite gene-activator protein: Structure, homology with other proteins, and cyclic AMP and DNA binding. Cold spring Harbor Symp. Quant. Biol. 47:419–426, 1983.